Atmos. Chem. Phys. Discuss., 15, 7933–7975, 2015
www.atmos-chem-phys-discuss.net/15/7933/2015/
doi:10.5194/acpd-15-7933-2015

Atmospheric Chemistry and Physics Discussions
Open Access

Utilization of O_4 slant column density to derive aerosol layer height from a spaceborne UV-visible hyperspectral sensor: sensitivity and case study

S. S. Park[1], J. Kim[1], H. Lee[1,2], O. Torres[3], K.-M. Lee[4], and S. D. Lee[5]

[1]Department of Atmospheric Science, Yonsei University, Seoul, Korea
[2]Department of Spatial Information Engineering, Pukyong National University, Busan, Korea
[3]NASA Goddard Space Flight Center, Greenbelt, Maryland, USA
[4]Department of Astronomy and Atmospheric Science, Kyungpook National University, Daegu, Korea
[5]National Institute of Environment Research, Ministry of Environment, Incheon, Korea

Received: 24 October 2014 – Accepted: 5 March 2015 – Published: 17 March 2015

Correspondence to: J. Kim (jkim2@yonsei.ac.kr)

Published by Copernicus Publications on behalf of the European Geosciences Union.

Utilization of O_4 slant column density to derive aerosol layer height

Abstract

The sensitivities of oxygen-dimer (O_4) slant column densities (SCDs) to changes in aerosol layer height are investigated using simulated radiances by a radiative transfer model, Linearized Discrete Ordinate Radiative Transfer (LIDORT), and Differential Optical Absorption Spectroscopy (DOAS) technique. The sensitivities of the O_4 SCDs to aerosol types and optical properties are also evaluated and compared. Among the O_4 absorption bands at 340, 360, 380, and 477 nm, the O_4 absorption band at 477 nm is found to be the most suitable to retrieve the aerosol effective height. However, the O_4 SCD at 477 nm is significantly influenced not only by the aerosol layer effective height but also by aerosol vertical profiles, optical properties including single scattering albedo (SSA), aerosol optical depth (AOD), and surface albedo. Overall, the error of the retrieved aerosol effective height is estimated to be 414 m (16.5 %), 564 m (22.4 %), and 1343 m (52.5 %) for absorbing, dust, and non-absorbing aerosol, respectively, assuming knowledge on the aerosol vertical distribution type. Using radiance data from the Ozone Monitoring Instrument (OMI), a new algorithm is developed to derive the aerosol effective height over East Asia after the determination of the aerosol type and AOD from the MODerate resolution Imaging Spectroradiometer (MODIS). The retrieved aerosol effective heights are lower by approximately 300 m (27 %) compared to those obtained from the ground-based LIDAR measurements.

1 Introduction

Aerosol is one of the key atmospheric constituents in understanding climate changes with its effects on direct and diffuse solar radiation (e.g., Haywood and Shine, 1995; Kaufman et al., 2002), and plays an important role in air quality near the surface (e.g., Watson et al., 1994; Prospero, 1999). For these reasons, observations from satellite remote sensing have been carried out to investigate aerosol properties in regional and global scale, including aerosol optical depth (AOD) (e.g., Curier et al., 2008; Levy et al.,

ACPD
15, 7933–7975, 2015

2007; Torres et al., 2007; Ahn et al., 2014; Veefkind et al., 1999; Zhang et al., 2011), fine mode fraction (FMF) or Angstrom Exponent (AE) (e.g., Jones and Christopher, 2007; Lee et al., 2010; Nakajima and Higurashi, 1998; Remer et al., 2008), single scattering albedo (SSA) (e.g., Dubovik et al., 2002; Levy et al., 2007; Jeong and Hsu, 2008; Torres et al., 1998, 2005, 2007; Jethva et al., 2014), and aerosol types (e.g., Higurashi and Nakajima, 2002; Kim et al., 2007; Lee et al., 2010). These information were further utilized to estimate radiative forcing of aerosol (e.g., Christopher et al., 2006; Chung et al., 2005; Chou et al., 2002), to understand the mechanism of the changes to the cloud formation (Twomey et al., 1984; Albrecht, 1989; Jones et al., 1994), and to monitor air quality (e.g., Wang and Christopher, 2003; Hutchison et al., 2005).

Vertical structures of atmospheric aerosols are affected by processes of formation, transport and deposition, and vary for different aerosol types over East Asia (Shimizu et al., 2004). Labonne et al. (2007) also reported that the layer top height of biomass burning aerosol ranged from 1.5 to 7 km in the wild fire regions. The information on the aerosol layer height is important, because the variation of the aerosol vertical distribution affects radiative process in the atmosphere near the surface. Uncertainty in aerosol layer height also affects the accuracy of aerosol AOD and SSA retrieval algorithms that use near UV observations (Torres et al., 1998, 2007; Jethva et al., 2014) and complicates the interpretation of the Aerosol Index (AI), a qualitative parameter commonly used to detect absorbing aerosols (Herman et al., 1997; Torres et al., 1998). In addition, there have been difficulties to estimate surface concentration of aerosol from AODs, because the information on aerosol vertical distribution is not readily available and even hard to predict from the state-of-the-art models due to its large variability. Although the Cloud-Aerosol Lidar with Orthogonal Polarization (CALIOP) have been successful and provided vertical structures of aerosols, its spatial coverage was very limited with its measurement characteristics (Omar et al., 2009). Liu et al. (2005) showed that the Particulate Matter (PM) concentration estimated by the AOD from satellite observation accounted for only 48 % of the measured surface PM, although their study reflected

ACPD
15, 7933–7975, 2015

variations of the aerosol types and its hygroscopic growth in the algorithms. One of the essential factors to consider in estimating PM from AOD is the vertical structure of aerosols (e.g. Chu, 2006; Seo et al., 2014). Therefore, conventional aerosol products would benefit significantly with the development of robust algorithm to retrieve aerosol height using satellite data.

The Differential Optical Absorption Spectroscopy (DOAS) technique has been used widely to retrieve trace gas concentration both from ground-based (e.g., Platt, 1994; Platt and Stutz, 2008) and space-borne (e.g., Wagner et al., 2010) measurements. Recently, several studies (e.g., Wagner et al., 2004; Friess et al., 2006; Irie et al., 2009, 2011; Lee et al., 2009, 2011; Clemer et al., 2010; Li et al., 2010) provided aerosol profiles from ground-based hyperspectral measurements in UV and visible wavelength ranges. Wagner et al. (2010) investigated the sensitivity of various factors to the aerosol layer height using the data obtained from the SCanning Imaging Absorption SpectroMeter for Atmospheric ChartographY (SCIAMACHY) on ENVISAT. The sensitivity of the Ring effect and the absorption by oxygen molecule (O_2) and its dimer (O_4) calculated by DOAS method were examined to estimate aerosol properties including the layer height. Kokhanovsky and Rozanov (2010) estimated dust altitudes using the O_2-A band between 760 and 765 nm after the determination of the dust optical depth. In addition, several previous studies are also investigated estimation methods for aerosol height information by using hyperspectral measurement in visible (e.g., Dubuisson et al., 2009; Koppers et al., 1997; Sanders and de Haan, 2013; Sanghavi et al., 2012; Wang et al., 2012). Because in the near UV the surface signal is significantly smaller than the aerosol signal, the UV and near UV regions are useful to derive aerosol height information from space borne measurements.

For OMI measurement, the O_4 band at 477 nm has been widely applied to estimate cloud information (e.g., Accarreta et al., 2004; Sneep et al., 2008). Furthermore, Veihelmann et al. (2007) introduced that the 477 nm channel, which locates major O_4 band, significantly adds degree of freedom for aerosol retrieval by using principal com-

ACPD
15, 7933–7975, 2015

ponent analysis, and Dirksen et al. (2009) adopts pressures from OMI O_4 band to study a plume height for aerosol transport cases.

In this study, the sensitivities of the O_4 bands at 340, 360, 380, and 477 nm to changes in aerosol layer height and its optical properties are estimated using simulated hyperspectral radiances, differently from the previous studies using the O_2-A band observation (e.g., Kokhanovsky and Rozanov, 2010). We proposed an improved DOAS algorithm for the O_4 absorption bands to retrieve aerosol height information from the O_4 slant column densities (SCDs) based on the sensitivity studies. This new algorithm is applied to the radiance data from the Ozone Monitoring Instrument (OMI) to retrieve the aerosol effective height (AEH) for a real case over East Asia, including error estimates.

2 Methods

In general, scattering by aerosol at low altitudes leads to an increase in the path length of light (albedo effect), while those at high altitudes causes a decrease in the path length of light (shielding effect) (Wagner et al., 2010). These two opposing effects change the estimated O_4 SCD values. Furthermore, the measured O_4 SCD is a function of wavelength, because the absorption and scattering by atmospheric molecules and aerosol have spectral dependence. Therefore, radiative transfer calculations are carried out to estimate the sensitivity of the O_4 SCD with respect to the change of atmospheric conditions. Details of the radiative transfer model (RTM) and input parameters to simulate radiance are discussed in Sect. 2.1. Analytical method of the DOAS to estimate the O_4 SCD is described in Sect. 2.2.

2.1 Simulation of hyperspectral radiance

Figure 1 shows the flowchart of the method to estimate the O_4 SCD from the simulated radiance. In order to investigate the sensitivities of the O_4 SCD at several bands in UV and visible wavelengths with respect to various aerosol properties, including AEHs, aerosol amounts and aerosol types, the hyperspectral radiance is simulated using the Linearlized Discrete Ordinate Radiative Transfer (LIDORT) model (Spurr et al., 2001; Spurr, 2002). The LIDORT model is suitable for the off-nadir satellite viewing geometry of passive sensors since this model adopts the spherically curved atmosphere to reflect the pseudo-spherical direct-beam attenuation effect (Spurr et al., 2001). The model calculates the monochromatic radiance ranging from 300 to 500 nm with a spectral resolution of 0.1 nm. The radiance spectrum is calculated with a 0.2 nm sampling resolution applying a slit response function (SRF) given by a normalized Gaussian distribution with 0.6 nm as the full-width half maximum (FWHM).

2.1.1 Aerosol properties

The aerosol input parameters for the RTM are important in simulating the radiance spectra because aerosol optical properties determine scattering and absorption characteristics. The data from the Optical Properties of Aerosol and Cloud (OPAC) package (Hess et al., 1998) are used as aerosol parameters, which includes the spectral complex refractive indices and size distribution of aerosols, to calculate SSA and phase function through the Mie calculations. Although the AERONET observation provides those aerosol parameters in the visible, they are not available at the UV wavelengths.

In terms of the aerosol types, water soluble (WASO), mineral dust (MITR), and continental polluted (COPO) model to simulate non-absorbing aerosol, mineral dust, and absorbing anthropogenic aerosol, respectively. The COPO is combined type that includes both soot and WASO, which represents the pure black-carbon and non-absorbing aerosols, respectively. The mixture of these two types, adequately describes the fine mode aerosol from anthropogenic pollution. The SSA is the largest for WASO and the smallest for COPO. In order to account for hygroscopic growth, the default relative humidity is assumed to be 80 % (c.f., Holzer-Popp and Schroedter-Homscheidt, 2004).

Discussion Paper | Discussion Paper | Discussion Paper | Discussion Paper |

ACPD

15, 7933–7975, 2015

Utilization of O_4 slant column density to derive aerosol layer height

S. S. Park et al.

2.1.2 Aerosol vertical distribution

In this study, "aerosol height" refers to AEH, defined as the altitude at which the aerosol extinction coefficient integrated from the surface is $(1 - e^{-1})$ of the AOD. According to Hayasaka et al. (2007), which introduced the AEH, the aerosol extinction coefficient was found to exponentially decrease with altitude over East Asia based on the ground-based LIDAR observation data during the Atmospheric Brown Clouds-East Asia Regional Experiment 2005 (ABC-EAREX 2005) campaign. Previous studies used the exponentially decreasing pattern with altitude to represent the aerosol vertical profiles (e.g. Hayasaka et al., 2007; Li et al., 2010), and reported that aerosol is present within 5 km in altitude for most of the cases (e.g. Sasano, 1996; Chiang et al., 2007). In particular, the AEH ranges from 1 to 5 km for 95 % of the cases over East Asia (Hayasaka et al., 2007), and ranges from 0.5 to 2.0 km over southern China (Li et al., 2010). From these previous studies, aerosol vertical distributions are assumed to be exponential with the AEHs ranging from 1 to 5 km for the RTM simulation here.

2.1.3 Trace gases

Table 1 summarizes the absorption cross sections of trace gases used as inputs for the radiance simulations and the DOAS spectral analysis technique. At wavelengths 340, 360, 380, and 477 nm, the O_4 absorption cross section values suggested by Hermans et al. (1999) are used. O_3 absorption cross sections at three different temperatures (223, 243, and 273 K) and NO_2 absorption cross sections at two different temperatures (220 and 294 K) are used to account for the amounts in the stratosphere and the troposphere. The vertical distribution of the O_4 number density, which is used to calculate its SCD from the RTM, has been assumed to be the square of the O_2 number density in each layer (Hermans et al., 2003). Thus, the total number of the O_4 column density from surface to TOA is 1.38×10^{43} molecule^2 cm^{-5}, where 93 and 73 % of the total O_4 is distributed below the altitude of 10 and 5 km, respectively. In particular, signals by the changes of O_4 SCD are strong below 5 km, where aerosol transports are observed fre-

ACPD
15, 7933–7975, 2015

quently. The vertical distributions of other atmospheric components are taken from the US standard atmosphere 1976 (United States Committee on Extension to the Standard Atmosphere, 1976). The vertical distribution of trace gases and aerosol in the troposphere are interpolated in the 0.1 km resolution from the sea level to 5 km.

2.2 DOAS analysis

The radiance information obtained from both the RTM simulation and from OMI measurements are analyzed to derive the O_4 SCDs using WinDOAS software (Van Roozendael and Fayt, 2001). To analyze the simulated radiances, the spectrum calculated without all atmospheric gases and aerosol are used as the Fraunhofer reference spectrum (FRS), while the irradiance spectrum (OML1BIRR) is used as the FRS for the analysis of OMI observed data. The simulated spectra are fitted simultaneously with the absorption cross sections of all trace gases listed in Table 1 and FRS in the respective wavelength range of 335–350, 350–370, 370–390, and 460–486 nm, using a nonlinear least squares method (Platt and Stutz, 2008). Similarly, OMI measurement spectra are fitted with the Ring spectrum and the FRS in addition to the absorption cross sections in Table 1 in the same wavelength intervals. Before the fitting process, the NO_2 and O_3 spectra are I_0 corrected, and the Ring spectrum (Fish and Jones, 1995), accounting for the effects of the rotational Raman scattering due to air molecules, is calculated from the FRS using the WinDOAS software. After the fitting, the noise level is estimated to be on the order of 10^{-4} and 10^{-3} for the radiance spectrum from the RTM simulation and OMI at 477 nm, respectively.

Figure 2 shows the comparison of the 477 nm O_4 SCD between the inversion from a look-up table (LUT) with the dimension as in Table 2, and the standard OMI product, OMCLDO2 (e.g., Accarreta et al., 2004; Sneep et al., 2008), for aerosol and cloud free pixels in Year 2005. Although O_4 SCD is for the clear sky pixels, the AOD for the RTM simulation is assumed to be 0.15 at 500 nm with the effective height of 3 km, based on the climatological background AOD of 0.13 ~ 0.14 at 550 nm from the MODIS observation over ocean (Remer et al., 2008). The clear sky region is selected for latitudes from 25 to 50° N and the longitudes from 170 to 180° E with cloud fraction less than 0.02 from OMI observation. Because the standard product of the O_4 SCD is only estimated at the 477 nm band, the results can be compared only for this band. To minimize the error from the DOAS fitting, the observed data from OMI is selected by the fitting precision less than 2 % and the quality flags for spectral fitting and pixel condition, are considered. As shown in Fig. 2a, the correlation coefficient of determination (R^2) is 0.878, with a slope of 1.214, and the LUT exhibits a ratio of 1.24 ± 0.04 to the values obtained from OMI standard values. Despite the statistically significant R^2 values between the two values, there exist positive bias by about 20 %, and the slope is greater than 1. The bias between the retrieved from LUT and estimated from standard product values can be attributed to the uncertainties in the absolute value of O_4 cross section database and the lack of their temperature and pressure dependence as noted from previous work of Wagner et al. (2009) and Clemer et al. (2010). To account for the difference between simulated and observed SCD, the correction factor of 1.25 to the O_4 cross section is used as suggested by Irie et al. (2011) and Lee et al. (2011). The corrected result is shown in Fig. 2b, where the R^2 is 0.880 similar to the value before the correction, but the positive ratio is reduced to 1.04 ± 0.04 and the regression line slope is improved to 1.135. Thus, the calculation by the LIDORT simulates the satellite observation and can be used for sensitivity tests to retrieve aerosol height.

3 Sensitivity test

3.1 Sensitivity of the O_4 SCDs to the AEH

The sensitivity of the O_4 SCD to the AEH is investigated for its absorption bands at 340, 360, 380, and 477 nm. Figures 3–6 show the O_4 SCD as a function of the AEH and the three different aerosol types of MITR, WASO and COPO at 340, 360, 380, and 477 nm, respectively. The vertical error bar represents the fitting error estimated by the noise spectra from the DOAS fitting (c.f. Stutz and Platt, 1996). For the calculation shown in

ACPD
15, 7933–7975, 2015

the figures, the following geometries are assumed: a solar zenith angle (SZA) of 30°, a viewing zenith angle (VZA) of 30°, and a relative azimuth angle (RAA) of 0°. In the four figures, the O_4 SCDs show the variations for the AEHs ranging from 1.0 to 5.0 km, and for the AODs of 0.4 and 1.0 at 500 nm. However, the absorbing aerosols in low AEH cases (AEH < 2 km) are largely fluctuated, and failed to fit due to large fitting error in 340, 360, and 380 nm. For this reason, the sensitivity result, which is defined the decrease rate of the O_4 SCD value in the 1 km interval of AEH ($-dO_4/dZ$), estimates in the AEH range of 2.0 to 4.0 km.

As shown in Fig. 3, the largest $-dO_4/dZ$ ranges from -3.1×10^{41} to 3.6×10^{42} molecule^2 cm^{-5} km^{-1}, which corresponds to −1.1 to 20.5 % of each binned O_4 SCD, depending on the aerosol types. The $-dO_4/dZ$ at 340 nm slightly increases as the AOD increases, due to the enhanced shield effect by the thick aerosol layer. Furthermore, the $-dO_4/dZ$ for the absorbing aerosol is larger than that for the non-absorbing aerosol, as the absorbing aerosol reduces the path length more effectively by its shielding effect than non-absorbing aerosol. However, the mean spectral fitting error of the O_4 SCD is estimated to be 2.1×10^{42} molecule^2 cm^{-5} km^{-1}, which is 2 times larger than the $-dO_4/dZ$. The large spectral fitting error is associated with the weak O_4 absorption at 340 nm. Furthermore, the unrealistic O_4 SCD value is estimated at low AEH cases (less than 1.5 km).

Similarly, the O_4 SCD is estimated at 360 nm band as shown in Fig. 4. The mean value of the $-dO_4/dZ$ is found to be in the range from 4.75×10^{41} to 2.76×10^{42} molecule^2 cm^{-5} km^{-1}, which corresponds to the relative difference ranging from 2.2 to 16.9 % of the estimated O_4 SCD. Moreover, the $-dO_4/dZ$ increases as the AOD increase and the SSA decrease. The $-dO_4/dZ$ for the AOD of 0.4 and 1.0 is 1.13×10^{42} and 1.61×10^{42} molecule^2 cm^{-5} km^{-1}, respectively. Furthermore, the $-dO_4/dZ$ is also calculated to be 1.21×10^{42}, 1.29×10^{42}, and 1.62×10^{42} molecule^2 cm^{-5} km^{-1} for the MITR, COPO, and WASO, respectively. The spectral fitting error is estimated to be 1.9 % of the total O_4 SCD, which is approximately 28 % for the $-dO_4/dZ$ at 360 nm. Therefore, this absorption band is considered to be useful in estimating the AEH. However, the fitting errors increased for SZA or VZA conditions larger than 50° and it also shows the impractical values at low AEH case. Similarly, the $-dO_4/dZ$ at the band of 380 nm is estimated to be in the range of 6.25×10^{41} to 2.70×10^{42} molecule^2 cm^{-5} km^{-1} as shown in Fig. 5. The relative difference is calculated to be 2.9 to 17.3 % of the simulated value of the total O_4 SCD, while the fitting error at the 380 nm band is 4.2 % of the total O_4 SCD. Therefore, this result indicates that the O_4 SCD difference with respect to the AEH change is insufficient to distinguish from the fitting error, which is the same order of the $-dO_4/dZ$.

Figure 6 shows the sensitivity of the O_4 SCD at 477 nm to the AEH changes. The $-dO_4/dZ$ is estimated to be 1.16×10^{42}, 1.21×10^{42}, and 0.98×10^{42} molecule^2 cm^{-5} km^{-1}, which corresponds to 4.1, 3.9, and 4.3 % of the total O_4 SCD for the MITR, WASO, and COPO, respectively, for the AOD of 0.4. The value for the AOD of 1.0 is estimated to be 1.63×10^{42}, 1.56×10^{42}, and 1.51×10^{42} molecule^2 cm^{-5} km^{-1}, which corresponds to 6.5, 5.1, and 8.5 % for the MITR, WASO, and COPO, respectively. The calculated $-dO_4/dZ$ are significantly larger than the mean fitting errors of 0.47 %, which implies that the O_4 SCD at 477 nm is useful in estimating the AEH. The small fitting errors at 477 nm are due to the larger O_4 absorption and less interferences by other trace gases in this spectral window. Although the retrieval error due to the spectral fitting is the largest for the MITR and the smallest for the COPO, the AEH retrieval error due to the spectral fitting corresponds to a value smaller than 100 m.

Table 3 shows the representative $-dO_4/dZ$ value as changing aerosol types in four absorption bands. In summary, the derived O_4 SCD varies as a function of the wavelength due to the spectral dependence of the aerosol optical properties and Rayleigh scattering effects. Considering the amplitude of the fitting errors compared to that of the $-dO_4/dZ$ in the O_4 absorption bands at 340, 360, and 380 nm, the variations in the O_4 SCDs with respect to the AEH changes are calculated not large enough to derive the AEH, while the O_4 SCD at 477 nm is considered to be the best candidate to derive the AEH due to the small fitting error and the large $-dO_4/dZ$. However, the

$-dO_4/dZ$ at 477 nm depends not only on the AEH, but also on the AOD and aerosol types, as shown in Fig. 6. Therefore, it is necessary to investigate the sensitivities of the O_4 SCDs at 477 nm to various AODs and aerosol types.

For different AODs (τ_a), the O_4 SCD at AEHs of 1.0 and 3.0 km is shown in Fig. 7 for the same geometry assumed in Figs. 3–6. The decreasing rate of the O_4 SCDs ($-dO_4/d\tau_a$) at 477 nm is found to be larger for the AEH of 3.0 km than for that of 1.0 km. Among the three aerosol types, the $-dO_4/d\tau_a$ is found to be the largest for the COPO, which has stronger absorbing characteristics than other two aerosol types. The mean $-dO_4/d\tau_a$ values are estimated to be 1.5, 2.7, and 0.1 % for the AEH of 1.0 km as the AOD changes by 0.2 in the MITR, COPO, and WASO, respectively, whereas they are estimated to be 3.3, 6.0, and 0.6 % for the AEH of 3.0 km with respect to the same AOD changes for the three different type, respectively.

Torres et al. (1998) showed that the result of the SSA from OMI can be overestimated due to the cloud contamination. Furthermore, the SSA varies widely as the categorizing aerosol types. Therefore, the sensitivity of O_4 SCDs to the SSA variation is estimated for the same geometries used in the previous tests. The O_4 SCDs at 477 nm change by 1.1 to 6.0 % for absorbing, and 2.0 to 10.5 % for non-absorbing aerosol with respect to 10 % of its SSA deviation. The difference is proportional to the absolute values of the SSA for all of the simulated cases.

Furthermore, as the surface albedo affects the $-dO_4/dZ$, the sensitivity of the O_4 SCD at 477 nm is also tested with respect to the surface albedo difference of 0.02. The difference of climatological surface albedo between that obtained from the total ozone monitoring spectrometer (TOMS) and the global ozone monitoring experiment (GOME) was known to be up to 0.02 (Koelemeijer et al., 2003). Table 4 shows the sensitivity of the O_4 SCDs at 477 nm with respect to the change in the surface albedo. The relative difference of O_4 SCD due to the surface albedo variation ranges from 0.76 to 2.62 % with uncertainties indicated. Furthermore, it is found that the difference of O_4 SCD due to surface albedo changes is higher for the absorbing aerosol than the non-absorbing

ACPD
15, 7933–7975, 2015

aerosol, which can be explained by the albedo effect to the O_4 SCD is larger for the absorbing aerosol.

3.2 Error analysis

Errors are also estimated in terms of previously tested variables in the retrieval of the O_4 SCD at 477 nm, with the variables and their dimensions as summarized in Table 5. Table 6 shows the summary of the total error budget for the AEH derivation with a list of the major error sources and their values, for the errors of each variable in OMI standard products. Because the differences in the O_4 SCD at 477 nm are not linearly correlated with the changes in AEH, the estimation error is modified from the column density units to the height. To convert the O_4 SCD difference to the AEH error, the difference of O_4 SCD due to the respective error source is divided by that from the change of the AEH in each bin of the AOD and AEH.

The mean errors from 10 % variation in the SSA for all of the variable conditions in Table 5 are calculated to be 27, 9, and 85 % for the MITR, COPO, and WASO, respectively. This mean error corresponds to 670, 230, and 2150 m for the MITR, COPO, and WASO, respectively. For the total error budget calculations, however, 5 % change in the SSA was used according to Torres et al. (2007), which reported that the variation of the SSA is less than 0.03 for the given aerosol types. Another important error source is the aerosol profile shape. The error from the vertical distribution is estimated to be 630, 430, and 1670 m for the COPO, MITR and WASO, respectively, which corresponds to the relative errors of AEH ranging from 17 to 66 %.

The errors from the SSA and the aerosol profile shape are the two important error sources in estimating the AEH, followed by the errors related to the AOD and the surface albedo. From OMI standard products, the expected error of the AOD is 0.1 (or 30 %), and 0.1 (or 20 %) for the absorbing and the non-absorbing aerosol over ocean, respectively. From these results, the errors of the AEH due to the error from OMI AOD of 0.2 and the surface albedo of 0.02 are less than 200 m. The mean error due to the uncertainty in the AOD is estimated to be 7.7, 7.1, and 6.6 % for the COPO, MITR,

ACPD
15, 7933–7975, 2015

and WASO, respectively, whereas that due to the uncertainty in the surface albedo is respectively estimated to be 4.1, 1.9, and 3.1 % for the COPO, MITR, and WASO.

In addition, the errors in the O_4 SCD, and thereby the AEH, are associated with the variations in the column amounts and the differences in the absorption cross section of each fitted trace gas for the spectral analysis. The variations in the column amounts of trace gases and the differences in the absorption cross section values do not affect significantly in calculating the O_4 SCD at 477 nm. However, the O_4 vertical column density is changed by the change in atmospheric pressure. In East Asia, the surface pressure over ocean is 1010.9±29.6 (3-sigma) hPa from NCEP Reanalysis 2 data since 2004. In clear case, the difference of O_4 SCD due to the ±3 % for pressure variation is 3.4 ± 0.1 % in all geometries, which is about half of the difference due to the uncertainty of 0.2 in AOD.

Furthermore, the AEH error in terms of inaccurate spectral wavelength calibration is estimated based on the assumed errors of ±0.02 nm, which corresponds to 0.1 pixels for OMI. Although it is well known that the accuracy in the spectral wavelength calibration before the DOAS fitting affects the trace gas SCD retrieval, the errors in the O_4 SCD at 477 nm associated with the wavelength shift of the sub-pixel scale are estimated to be negligible due to the broad O_4 absorption band width around 477 nm. Overall, the total error budget in the AEH retrieval is estimated to be 16.5 (414 m), 22.4 (564 m), and 52.5 % (1343 m) for the COPO, MITR, and WASO, respectively, with the exception of the contribution of the errors in the aerosol vertical profiles.

This study uses the AEH for the exponential vertical distribution of aerosols as described in Sect. 2.1.2. However, aerosol layers are often elevated above the planetary boundary layer (PBL) as a result of long-range transport for which the vertical distribution of aerosol can be better described by Gaussian shape. Therefore, the sensitivity in the O_4 SCDs is tested for the two vertical profiles. Table 7 shows the differences in the O_4 SCDs between the two vertical profiles of aerosol assumed, with the variables and their dimensions as listed in Table 5. The estimated errors caused solely by the change between the two aerosol vertical profiles, range from −13.27 to 8.97 %. Therefore, the aerosol vertical distribution is one of the major error sources to estimate the AEH. From the column density units to the height, the estimation error of AEH due to aerosol vertical distribution is 433, 634, and 1669 m for the MITR, COPO, and WASO, respectively.

4 Case study

To demonstrate the feasibility from real measurements, the AEHs are derived using hyperspectral data from OMI. OMI channels are composed of UV-1 (270–314 nm), UV-2 (306–380 nm), and a visible wavelength range (365–500 nm) with a spectral resolution (FWHM) of 0.63, 0.42, and 0.63 nm, respectively (Levelt et al., 2006). The spatial resolution is 13 km × 24 km at nadir in "Global Mode". In the present study, the spectral data over the visible wavelength range are used to derive the O_4 SCD at 477 nm and the AEH information.

Figure 8 describes an algorithm for the AEH derivation for the case study. In retrieving AEH, AOD, FMF and the aerosol types are obtained from a separated algorithm using the MODIS 4 channel algorithm as described by Kim et al. (2007) (4CA hereafter) due to simultaneously provide accurate result of aerosol types. After determining AOD, FMF, and aerosol types, LUT, which is generated as functions of geometries (SZA, VZA, and RAA), aerosol types and AODs, is used to determine the AEH information by using comparison between simulated and measured O_4 SCD value. The variables and their dimensions for the LUT calculations are shown in Table 8. Due to the limitation of the accuracy of aerosol type classification and those of AOD over land, this study only estimates the AEH over ocean surface. Because the temporal and spatial variation of surface albedo over ocean is less than 0.02, the climatological value from OMI Level 3 (OMLER) is used in this study (Kleipool et al., 2008). Although the error for the surface albedo affects the AEH retrieval, the retrieval error for the surface albedo is less than 100 m from the error analysis as shown in Table 6.

ACPD
15, 7933–7975, 2015

By using the observed radiance data from OMI, the AEH is estimated for the transported dust case. Figure 9 shows the results of the retrieved AEH during the Asian dust event on 31 March 2007. MODIS 4CA products of AOD and aerosol type on this date show that thick dust layer with the AOD up to 1.0 is observed from China to the Yellow sea (Fig. 9b) and the FMF ranging from 0.2 to 0.4, indicating the dominance of coarse-mode particles (Fig. 9c). The aerosol type over the Yellow Sea is classified as dust type (yellow color) (Fig. 9d). Using the basis of the prototype algorithm with the pre-determined AOD and type, the mean retrieved AEH is 2.6 ± 1.7 km over 1633 pixels in East Asia (Fig. 9e). The retrieved result is compared with the backscattering intensity from CALIOP observation over Yellow sea and the backscattering signal of the ground-based LIDAR data at a site in Seoul (Seoul National University, 37.45° N, 126.95° E, altitude: 118 m) as shown in Fig. 10. From CALIOP observation, the aerosol layer height over Yellow sea is located 1.0 ~ 1.5 km altitude for most observed regions. Over the Yellow sea domain in 35 ~ 40° N and 120 ~ 130° E, the AEH from OMI is 1.7 ± 1.3 km over 166 pixels, which is within 1 km difference from CALIOP. The AEH obtained from the LIDAR measurement is estimated to be 0.9 ± 0.3 km, according to the same definition in Sect. 2.1.2. Because of the cloudy condition over the west coast of the Korean Peninsula region at the satellite overpass time as shown in Fig. 9a, the observed signal from the LIDAR is saturated by the clouds at the layer below 1 km in the morning. After removing the saturated backscattering signal by the clouds, the AEH obtained from the LIDAR is calculated to be 1.1 ± 0.1 km. Then, the estimated AEH derived from OMI data near the LIDAR site within ±1.5° is 0.8 ± 0.7 km at 11 pixels as shown in Fig. 9f. It should be noted that the SD of the AEH from the LIDAR and OMI respectively indicates the temporal and spatial variation of the AEH. From the retrieved result, the retrieved AEH is underestimated by 27 %, and the investigated algorithm quantitatively estimates the AEH over East Asia. Furthermore, the retrieved error ranges within 27 % is still meaningful considering the total error budget suggested from the error analysis, 22.4 ± 19.8 % for dust.

ACPD
15, 7933–7975, 2015

5 Summary and discussion

The sensitivities of the O_4 SCD at 340, 360, 380, and 477 nm bands are investigated with RTM calculations to derive the AEH using the space-borne hyperspectral data. Among these O_4 absorption bands, the O_4 SCD at 477 nm is considered to be suitable for the AEH retrieval. In addition to the AEH, AOD, aerosol type, aerosol vertical profile, and surface albedo are also found to have effects on the O_4 SCD at 477 nm, while the spectral calibration and cross section of the atmospheric gases have negligible effects on the O_4 SCD. The major error source for the AEH retrieval is the SSA variation, which leads to the AEH error ranging from 9 to 85 % with the SSA variation by 10 %. In addition, the profile shape is also a major error source for the AEH estimation. According to the error estimations, the total errors are 414 m (16.5 %), 564 m (22.4 %), and 1343 m (52.5 %) for absorbing, dust, and non-absorbing aerosol, respectively, due to uncertainties of the variation from AOD, SSA, and surface albedo.

In addition to the sensitivity analysis, an algorithm for the AEH derivation is developed for the first time based on a LUT that consists of the O_4 SCD at 477 nm in terms of the AEH, AOD, aerosol types, surface albedo, and measurement geometries. After the determination of AOD and aerosol types from the MODIS 4CA, the AEH value is derived over East Asia via application of the algorithm to OMI measurement data. To consider the accuracy of the AOD and the aerosol types, the result is shown over ocean surface. From the case for the dust, the derived AEH shows significant value as compared to aerosol layer height from CALIOP, and lower values than the result from the ground-based LIDAR in Seoul by 300 m (27 %), which is within the magnitude of estimated error.

There are many works to be done to improve the newly introduced algorithm as it requires the products from MODIS to determine the AOD and aerosol types before the AEH retrieval. The vertical distribution and the optical properties of the aerosol need to be quantified using the observation database, such as MPLNET and AERONET. Furthermore, the spatial variation of the AOD, surface pressure and the contamination

ACPD
15, 7933–7975, 2015

by the cloud in the sub-pixel scale need to be investigated as they are also thought to affect the retrieved results. If the surface reflectance can be characterized with sufficient accuracy, the retrieval of the AEH can be extended to over land. In addition, the O_4 SCD method in this study can be applied to the surface pressure estimation in clear regions.

Acknowledgements. This work was supported by the Eco Innovation Program of KEITI (ARQ201 204 015), Korea, and it was also supported by the Brain Korea plus program.

References

Ahn, C., Torres, O., and Jethva, H.: Assessment of OMI near-UV aerosol optical depth over land, J. Geophys. Res., 119, 2457–2473, doi:10.1002/2013JD020188, 2014.

Albrecht, B. A.: Aerosols, cloud microphysics, and fractional cloudiness, Science, 245, 1227–1230, 1989.

Bogumil, K., Orphal, J., Burrows, J. P., and Flaud, J. M.: Vibrational progressions in the visible and near-ultraviolet absorption spectrum of ozone, Chem. Phys. Lett., 349, 241–248, 2001.

Chiang, C.-W., Chen, W.-N., Liang, W.-A., Das, S. K., and Nee, J.-B.: Optical properties of tropospheric aerosols based on measurements of lidar, sun-photometer and visibility at Chung-Li (25° N, 121° E), Atmos. Environ., 41, 4128–4137, 2007.

Chou, M.-D, Chan, P.-K., and Wang, M.: Aerosol radiative forcing derived from SeaWiFS-retrieved aerosol optical properties, J. Atmos. Sci., 59, 748–757, 2002.

Christopher, S. A., Zhang, J., Kaufman, Y. J., and Remer, L. A.: Satellite-based assessment of top of atmosphere anthropogenic aerosol radiative forcing over cloud-free oceans, Geophys. Res. Lett., 33, L15816, doi:10.1029/2005GL025535, 2006.

Chu, D. A.: Analysis of the Relationship Between MODIS Aerosol Optical Depth and $PM_{2.5}$ in the Summertime US, Optics & Photonics, International Society for Optics and Photonics, Proc. SPIE, Remote Sensing of Aerosol and Chemical Gases, Model Simulation/Assimilation, and Applications to Air Quality, San Diego, CA, 6299, 629903–629909, doi:10.1117/12.678841, 2006.

Chung, E. C., Ramanathan, V., Kim, D., and Podgorny. I. A.: Global anthropogenic aerosol direct forcing derived from satellite and ground-based observations, J. Geophys. Res., 110, D24207, doi:10.1029/2005JD006356, 2005.

Clémer, K., Van Roozendael, M., Fayt, C., Hendrick, F., Hermans, C., Pinardi, G., Spurr, R., Wang, P., and De Mazière, M.: Multiple wavelength retrieval of tropospheric aerosol optical properties from MAXDOAS measurements in Beijing, Atmos. Meas. Tech., 3, 863–878, doi:10.5194/amt-3-863-2010, 2010.

Curier, R. L., Veefkind, J. P., Braak, R., Veihelmann, B., Torres, O., and de Leeuw, G.: Retrieval of aerosol optical properties from OMI radiances using a multiwavelength algorithm: application to western Europe, J. Geophys. Res., 113, D17S90, doi:10.1029/2007JD008738, 2008.

Dirksen, R. J., Boersma, K. F., de Laat, J., Stammes, P., van der Werf, G. R., Martin, M. V., and Kelder, H. M.: An aerosol boomerang: rapid around-the-world transport of smoke from the December 2006 Australian forest fires observed from space, J. Geophys. Res., 114, D21201, doi:10.1029/2009JD012360, 2009.

Dubovik, O., Holben, B., Eck, T. F., Smirnov, A., Kaufman, Y. J., King, M. D., Tanre, D., and Slutsker, I.: Variability of absorption and optical properties of key aerosol types observed in worldwide locations, J. Atmos. Sci., 59, 590–608, 2002.

Dubuisson, P., Frouin, R., Dessaily, D., Duforet, L., Leon, J.-F., Voss, K., and Antoine, D.: Estimating the altitude of aerosol plumes over the ocean from reflectance ratio measurements in the O_2 A-band, Remote Sens. Environ., 113, 1899–1911, doi:10.1016/j.rse.2009.04.018, 2009.

Fish, D. J. and Jones, R. L.: Rotational Raman scattering and the ring effect in zenith-sky spectra, Geophys. Res. Lett., 22, 811–814, 1995.

Friess, U., Monk, P. S., Remedios, J. J., Rozanov, A., Sinreich, R., Wagner, T., and Platt, U.: MAX-DOAS O_4 measurements: a new technique to derive information on atmospheric aerosols: 2. Modeling studies, J. Geophys. Res., 111, D14203, doi:10.1029/2005JD006618, 2006.

Hayasaka, T., Satake, S., Shimizu, A., Sugimoto, N., Matsui, I., Aoki, K., and Muraji, Y.: Vertical distribution and optical properties of aerosols observed over Japan during the Atmospheric Brown Clouds-East Asia Regional Experiment 2005, J. Geophys. Res., 112, D22S35, doi:10.1029/2006JD008086, 2007.

Haywood, J. M. and Shine, K. P.: The effect of anthropogenic sulfate and soot aerosol on the clear sky planetary radiation budget, Geophys. Res. Lett., 22, 603–606, 1995.

ACPD
15, 7933–7975, 2015

Herman, J. R., Bhartia, P. K., Torres, O., Hsu, C., Seftor, C., and Celarier, E.: Global distribution of UV-absorbing aerosols from Nimbus-7/TOMS data, J. Geophys. Res., 102, 16911–16922, 1997.
Hermans, C., Vandaele, A. C., Carleer, M., Fally, S., Colin, R., Jenouvrier, A., Coquart, B., and Merienne, M.: Absorption cross-sections of atmospheric constituents: NO_2, O_2, and H_2O, Environ. Sci. Pollut. R., 6, 151–158, 1999.
Hermans, C., Vandaele, A. C., Fally, S., Carleer, M., Colin, R., Coquart, B., Jenouvrier, A., and Merienne, M. F.: Absorption cross-section of the collision-induced bands of oxygen from the UV to the NIR, in: Weakly Interacting Molecular Pairs: Unconventional Absorbers of Radiation in the Atmosphere, Springer, the Netherlands, 193–202, 2003.
Hess, M., Koepke, P., and Schult, I.: Optical properties of aerosols and clouds: the software package OPAC, B. Am. Meteorol. Soc., 79, 831–844, 1998.
Higurashi, A. and Nakajima, T.: Detection of aerosol types over the East China Sea near Japan from four-channel satellite data, Geophys. Res. Lett., 29, 1836, doi:10.1029/2002GL015357, 2002.
Holzer-Popp, T. and Schroedter-Homscheidt, M.: Synergetic aerosol retrieval from ENVISAT, in: Proc. ERS/ENVISAT Symposium, Salzburg, 6–10 September, Vol. 6, No. 10.9, 2004.
Hutchison, K. D., Smith, S., and Faruqui, S. J.: Correlating MODIS aerosol optical thickness data with ground-based $PM_{2.5}$ observations across Texas for use in a real-time air quality prediction system, Atmos. Environ., 39, 7190–7203, 2005.
Irie, H., Kanaya, Y., Akimoto, H., Iwabuchi, H., Shimizu, A., and Aoki, K.: Dual-wavelength aerosol vertical profile measurements by MAX-DOAS at Tsukuba, Japan, Atmos. Chem. Phys., 9, 2741–2749, doi:10.5194/acp-9-2741-2009, 2009.
Irie, H., Takashima, H., Kanaya, Y., Boersma, K. F., Gast, L., Wittrock, F., Brunner, D., Zhou, Y., and Van Roozendael, M.: Eight-component retrievals from ground-based MAX-DOAS observations, Atmos. Meas. Tech., 4, 1027–1044, doi:10.5194/amt-4-1027-2011, 2011.
Jeong, M.-J. and Hsu, N. C.: Retrievals of aerosol single-scattering albedo and effective aerosol layer height for biomass-burning smoke: synergy derived from “A-Train” sensors, Geophys. Res. Lett., 35, L24801, doi:10.1029/2008GL036279, 2008.
Jethva, H., Torres, O., and Ahn, C.: Global assessment of OMI aerosol single-scattering albedo using ground-based AERONET inversion, J. Geophys. Res., 119, 9020–9040, doi:10.1002/2014JD021672, 2014.

Jones, A., Roberts, D. L., and Slingo, A.: A climate model study of indirect radiative forcing by anthropogenic sulphate aerosols, Nature, 370, 450–453, 1994.
Jones, T. A. and Christopher, S. A.: MODIS derived fine mode fraction characteristics of marine, dust, and anthropogenic aerosols over the ocean, constrained by GOCART, MOPITT, and TOMS, J. Geophys. Res., 112, D22204, doi:10.1029/2007JD008974, 2007.
Kaufman, Y. J., Tanre, D., and Boucher, O.: A satellite view of aerosols in the climate system, Nature, 419, 215–223, 2002.
Kim, J., Lee, J., Lee, H. C., Higurashi, A., Takemura, T., and Song, C. H.: Consistency of the aerosol type classification from satellite remote sensing during the Atmospheric Brown Cloud – East Asia Regional Experiment campaign, J. Geophys. Res., 112, D22S33, doi:10.1029/2006JD008201, 2007.
Kleipool, Q. L., Dobber, M. R., de Haan, J. F., and Levelt, P. F.: Earth surface reflectance climatology from 3 years of OMI data, J. Geophys. Res., 113, D18308, doi:10.1029/2008JD010290, 2008.
Koelemeijer, R. B. A., de Haan, J. F., and Stammes, P.: A database of spectral surface reflectivity in the range 335–772 nm derived from 5.5 years of GOME observations, J. Geophys. Res., 108, 4070, doi:10.1029/2002JD002429, 2003.
Kokhanovsky, A. A. and Rozanov, V. V.: The determination of dust cloud altitudes from a satellite using hyperspectral measurements in the gaseous absorption band, Int. J. Remote Sens., 31, 2729–2744, 2010.
Koppers, G. A. A., Jansson, J., and Murtagh, D. P.: Aerosol optical thickness retrieval from GOME data in the oxygen A-band, ESA SP, 693–696, 1997.
Labonne, M., Breon, F.-M., and Chevallier, F.: Injection height of biomass burning aerosols as seen from a spacebornelidar, Geophys. Res. Lett., 34, L11806, doi:10.1029/2007GL029311, 2007.
Lee, H., Irie, H., Kim, Y. J., Noh, Y., Lee, C., Kim, Y., and Chun, K. J.: Retrieval of aerosol extinction in the lower troposphere based on UV MAX-DOAS measurements, Aerosol Sci. Tech., 43, 502–509, 2009.
Lee, H., Irie, H., Gu, M., Kim, J., and Hwang, J.: Remote sensing of tropospheric aerosol using UV MAX-DOAS during hazy conditions in winter: utilization of O_4 absorption bands at wavelength intervals of 338–368 and 367–393 nm, Atmos. Environ., 45, 5760–5769, doi:10.1016/j.atmosenv.2011.07.019, 2011.

Lee, J., Kim, J., Song, C. H., Ryu, J.-H., Ahn, Y.-H., and Song, C. K.: Algorithm for retrieval of aerosol optical properties over the ocean from the Geostationary Ocean Color Imager, Remote Sens. Environ., 114, 1077–1088, 2010.

Levelt, P. F., van den Oord, G. H. J., Dobber, M. R., Maelkki, A., Visser, H., de Vries, J., Stammes, P., Lundell, J. O. V., and Saari, H.: The Ozone Monitoring Instrument, IEEE T. Geosci. Remote, 44, 1093–1101, 2006.

Levy, R. C., Remer, L. A., Mattoo, S., Vermote, E. F., and Kaufman, Y. J.: Second-generation operational algorithm: retrieval of aerosol properties over land from inversion of Moderate Resolution Imaging Spectroradiometer spectral reflectance, J. Geophys. Res., 112, D13211, doi:10.1029/2006JD007811, 2007.

Li, X., Brauers, T., Shao, M., Garland, R. M., Wagner, T., Deutschmann, T., and Wahner, A.: MAX-DOAS measurements in southern China: retrieval of aerosol extinctions and validation using ground-based in-situ data, Atmos. Chem. Phys., 10, 2079–2089, doi:10.5194/acp-10-2079-2010, 2010.

Liu, Y., Sarnat, J. A., Kilaru, V., Jacob, D. J., and Koutrakis, P.: Estimating ground-level $PM_{2.5}$ in the Eastern United States using satellite remote sensing, Environ. Sci. Technol., 39, 3269–3278, 2005.

Nakajima, T. and Higurashi, A.: A use of two-channel radiances for and aerosol characterization from space, Geophys. Res. Lett., 25, 3815–3818, 1998.

Omar, A. H., Winker, D. M., Kittaka, C., Vaughan, M. A., Liu, Z., Hu, Y., Trepte, C. R., Rogers, R. R., Ferrare, R. A., Lee, K.-P., Kuehn, R. E., and Hostetler, C. A.: The CALIPSO automated aerosol classification and lidar ratio selection algorithm, J. Atmos. Ocean. Tech., 26, 1994–2014, 2009.

Platt, U.: Differential optical absorption spectroscopy (DOAS), air monitoring by spectroscopic technique, edited by: Sigrist, M. W., Chemical Analysis Series, Wiley, New York, 127, 27–84, 1994.

Platt, U. and Stutz, J.: Differential Absorption Spectroscopy, Springer, Berlin, Heidelberg, 2008.

Prospero, J. M.: Long-term measurements of the transport of African mineral dust to the southeastern United States: implications for regional air quality, J. Geophys. Res., 104, 15917–15927, 1999.

Remer, L. A., Kleidman, R. G., Levy, R. C., Kaufman, Y. J., Tanre, D., Mattoo, S., Martins, J. V., Ichoku, C., Koren, I., Yu, H., and Holben, B. N.: Global aerosol climatology from the MODIS satellite sensors, J. Geophys. Res., 113, D14S07, doi:10.1029/2007JD009661, 2008.

ACPD
15, 7933–7975, 2015

Sanders, A. F. J. and de Haan, J. F.: Retrieval of aerosol parameters from the oxygen A band in the presence of chlorophyll fluorescence, Atmos. Meas. Tech., 6, 2725–2740, doi:10.5194/amt-6-2725-2013, 2013.

Sanghavi, S., Martonchik, J. V., Landgraf, J., and Platt, U.: Retrieval of the optical depth and vertical distribution of particulate scatterers in the atmosphere using O_2 A- and B-band SCIAMACHY observations over Kanpur: a case study, Atmos. Meas. Tech., 5, 1099–1119, doi:10.5194/amt-5-1099-2012, 2012.

Sasano, Y.: Tropospheric aerosol extinction coefficient profiles derived from scanning lidar measurements over Tsukuba, Japan, from 1990 to 1993, Appl. Optics, 35, 4941–4952, 1996.

Seo, S., Kim, J., Lee, H., Jeong, U., Kim, W., Holben, B. N., Kim, S.-W., Song, C. H., and Lim, J. H.: Estimation of PM_{10} concentrations over Seoul using multiple empirical models with AERONET and MODIS data collected during the DRAGON-Asia campaign, Atmos. Chem. Phys., 15, 319–334, doi:10.5194/acp-15-319-2015, 2015.

Shimizu, A., Sugimoto, N., Matsui, I., Arao, K., Uno, I., Murayama, T., Kagawa, N., Aoki, K., Uchiyama, A., and Yamazaki, A.: Continuous observation of Asian dust and other aerosols by polarization lidars in China and Japan during ACE-Asia, J. Geophys. Res., 109, D19S17, doi:10.1029/2002JD003253, 2004.

Spurr, R. J. D.: Simultaneous derivation of intensities and weighting functions in a general pseudo-spherical discrete ordinate radiative transfer treatment, J. Quant. Spectrosc. Ra., 75, 129–175, 2002.

Spurr, R. J. D., Kurosu, T. P., and Chance, K. V.: A linearized discrete ordinate radiative transfer model for atmospheric remote-sensing retrieval, J. Quant. Spectrosc. Ra., 68, 689–735, 2001.

Stutz, J. and Platt, U.: Numerical analysis and estimation of the statistical error of differential optical absorption spectroscopy measurements with least-squares methods, Appl. Optics, 35, 6041–6053, 1996.

Torres, O., Bhartia, P. K., Herman, J. R., Ahmad, Z., and Gleason, J.: Derivation of aerosol properties from satellite measurements of backscattered ultraviolet radiation: theoretical basis, J. Geophys. Res., 103, 17099–17110, 1998.

Torres, O., Bhartia, P. K., Sinyuk, A., Welton, E. J., and Holben, B. N.: Total Ozone Mapping Spectrometer measurements of aerosol absorption from space: comparison to SAFARI 2000 ground-based observations, J. Geophys. Res., 110, D10S18, doi:10.1029/2004JD004611, 2005.

ACPD
15, 7933–7975, 2015

Utilization of O_4 slant column density to derive aerosol layer height

S. S. Park et al.

Torres, O., Tanskanen, A., Veihelmann, B., Ahn, C., Braak, R., Bhartia, P. K., Veefkind, P., and Levelt, P.: Aerosols and surface UV products from Ozone Monitoring Instrument observations: an overview, J. Geophys. Res., 112, D24S47, doi:10.1029/2007JD008809, 2007.

Twomey, S. A., Piepgrass, M., and Wolfe, T. L.: An assessment of the impact of pollution on the global albedo, Tellus B, 36, 356–366, 1984.

United States Committee on Extension to the Standard Atmosphere: US Standard Atmosphere 1976, National Oceanic and Atmospheric Administration, NASA, United States Air Force, Washington DC, USA, 1976.

Van Roozendael, M. and Fayt, C.: WinDOAS 2.1 Software User Manual, IASB/BIRA, Uccle, 2001.

Vandaele, A. C., Hermans, C., Simon, P. C., Carleer, M., Colin, R., Fally, S., Merienne, M. F., Jenouvrier, A., and Coquart, B.: Measurements of the NO_2 absorption cross-section from 42 000 to 10 000 cm^{-1} (238–1000 nm) at 220 and 294 K, J. Quant. Spectrosc. Ra., 59, 171–184, 1998.

Veefkind, J. P., de Leeuw, G., Durkee, P. A., Russell, P. B., Hobbs, P. V., and Livingston, J. M.: Aerosol optical depth retrieval using ATSR-2 and AVHRR data during TARFOX, J. Geophys. Res., 104, 2253–2260, 1999.

Veihelmann, B., Levelt, P. F., Stammes, P., and Veefkind, J. P.: Simulation study of the aerosol information content in OMI spectral reflectance measurements, Atmos. Chem. Phys., 7, 3115–3127, doi:10.5194/acp-7-3115-2007, 2007.

Wagner, T., Dix, B., Friedeburg, C. V., Friess, U., Sanghavi, S., Sinreich, R., and Platt, U.: MAX-DOAS O_4 measurements: a new technique to derive information on atmospheric aerosols – principles and information content, J. Geophys. Res., 109, D22205, doi:10.1029/2004JD004904, 2004.

Wagner, T., Deutschmann, T., and Platt, U.: Determination of aerosol properties from MAX-DOAS observations of the Ring effect, Atmos. Meas. Tech., 2, 495–512, doi:10.5194/amt-2-495-2009, 2009.

Wagner, T., Beirle, S., Deutschmann, T., and Penning de Vries, M.: A sensitivity analysis of Ring effect to aerosol properties and comparison to satellite observations, Atmos. Meas. Tech., 3, 1723–1751, doi:10.5194/amt-3-1723-2010, 2010.

Wang, J. and Christopher, S. A.: Intercomparison between satellite-derived aerosol optical thickness and $PM_{2.5}$ mass: implications for air quality studies, Geophys. Res. Lett., 30, 2095, doi:10.1029/2003GL018174, 2003.

Wang, P., Tuinder, O. N. E., Tilstra, L. G., de Graaf, M., and Stammes, P.: Interpretation of FRESCO cloud retrievals in case of absorbing aerosol events, Atmos. Chem. Phys., 12, 9057–9077, doi:10.5194/acp-12-9057-2012, 2012.

Watson, J. G., Chow, J. C., Lu, Z., Fujita, E. M., Lowenthal, D. H., Lawson, D. R., and Ashbaugh, L. L.: Chemical mass balance source apportionment of PM_{10} during the Southern California air quality study, Aerosol Sci. Tech., 21, 1–36, 1994.

Zhang, H., Lyapustin, A., Wang, Y., Kondragunta, S., Laszlo, I., Ciren, P., and Hoff, R. M.: A multi-angle aerosol optical depth retrieval algorithm for geostationary satellite data over the United States, Atmos. Chem. Phys., 11, 11977–11991, doi:10.5194/acp-11-11977-2011, 2011.

ACPD

15, 7933–7975, 2015

Table 1. The database of cross section for DOAS fitting analysis.

Species	Temperature (K)	Reference
O_3	223, 243, and 273	Bogumil et al. (2001)
NO_2	220 and 294	Vandaele et al. (1998)
O_4	298	Hermans et al. (1999)*

* Correction factor of 1.25 is used for the simulation.

ACPD
15, 7933–7975, 2015

Utilization of O_4 slant column density to derive aerosol layer height

S. S. Park et al.

Table 2. Dimensions of LUT for the clear sky comparison.

Variable name	No. of Entries	Entries
SZA	7	0, 10, 20, 30, 40, 50, 60°
VZA	7	0, 10, 20, 30, 40, 50, 60°
RAA	10	0, 20, 40, 60, 80, 100, 120, 140, 160, 180°

SZA: solar zenith angle, VZA: viewing zenith angle, RAA: relative azimuth angle.

ACPD
15, 7933–7975, 2015

Utilization of O_4 slant column density to derive aerosol layer height

S. S. Park et al.

Table 3. Sensitivity of AEH ($-dO_4/dZ$) in four O_4 bands from the simulation.

$-dO_4/dZ$ (molecule^2 cm^{-5} km^{-1})	MITR	WASO	COPO
340 nm	1.29×10^{42}	1.83×10^{42}	1.52×10^{42}
360 nm	1.21×10^{42}	1.62×10^{42}	1.29×10^{42}
380 nm	1.31×10^{42}	1.33×10^{42}	1.61×10^{42}
477 nm	1.40×10^{42}	1.24×10^{42}	1.39×10^{42}

ACPD
15, 7933–7975, 2015

Table 4. The difference of O_4 SCD due to the variation of surface albedo in percentage.

Albedo (Reference: 0.03)	0.01	0.05
MITR	$-0.85 \pm 1.03\,\%$	$0.76 \pm 0.84\,\%$
WASO	$-0.81 \pm 0.66\,\%$	$0.78 \pm 0.57\,\%$
COPO	$-2.62 \pm 3.34\,\%$	$2.12 \pm 2.42\,\%$

ACPD
15, 7933–7975, 2015

Utilization of O_4 slant column density to derive aerosol layer height

S. S. Park et al.

Table 5. Dimensions of simulation cases for the error analysis of the AEH retrieval.

Variable name	No. of Entries	Entries
SZA	4	0, 20, 40, 60°
VZA	7	0, 10, 20, 30, 40, 50, 60°
RAA	6	0, 40, 60, 120, 140, 180°
AOD	5	0.4, 1.0, 1.6, 2.5, 3.0
AEH	8	1.0, 1.2, 1.6, 2.0, 2.4, 3.0, 4.0, 5.0 km
Aerosol Model	3	MITR, WASO, COPO

ACPD
15, 7933–7975, 2015

Table 6. Summary of error sources and total error budget for the AEH retrieval.

Error source	MITR	WASO	COPO
AOD (ΔAOD = 0.2)	180 ± 123 m	166 ± 113 m	195 ± 138 m
SSA (10 % change)	671 ± 551 m	2155 ± 1501 m[a]	229 ± 208 m
Surface Albedo ($\Delta\alpha = 0.02$)	48 ± 98 m	79 ± 93 m	104 ± 283 m
Atmospheric Gases		< 5 m	
Atmospheric Pressure[b] ($\Delta P = 3\,\%$)		3.4 ± 0.1 % (O_4 SCD)	
Instrument (Shift: 0.02 nm)		< 10 m	
Total Error	22.4 ± 19.8 % (564 m)	52.5 ± 38.0 % (1343 m)	16.5 ± 21.0 % (414 m)

[a] Calculation results for the SSA decrease of 10 %.
[b] For clear sky calculation.

Discussion Paper | Discussion Paper | Discussion Paper | Discussion Paper |

ACPD
15, 7933–7975, 2015

Utilization of O_4 slant column density to derive aerosol layer height

S. S. Park et al.

Table 7. The difference of O_4 SCD and error for AEH due to the change of aerosol vertical distribution.

Reference shape (Exponential)	MITR (Gaussian)	WASO (Gaussian)	COPO (Gaussian)
Difference of estimation [%]	−5.40 ± 10.24	−13.27 ± 10.98	8.97 ± 14.55
Error for AEH [m]	433 ± 1644	1669 ± 2492	634 ± 1096

ACPD
15, 7933–7975, 2015

Utilization of O_4 slant column density to derive aerosol layer height

S. S. Park et al.

Table 8. Dimensions of LUT for the AEH algorithm using OMI.

Variable name	No. of Entries	Entries
SZA	7	0, 10, 20, 30, 40, 50, 60°
VZA	7	0, 10, 20, 30, 40, 50, 60°
RAA	10	0, 20, 40, 60, 80, 100, 120, 140, 160, 180°
AOD	13	0.0, 0.2, 0.4, 0.6, 0.8, 1.0, 1.3, 1.6, 1.9, 2.2, 2.5, 3.0, 5.0
AEH	16	0.0, 1.0, 1.2, 1.4, 1.6, 1.8, 2.0, 2.2, 2.4, 2.6, 2.8, 3.0, 3.5, 4.0, 5.0, 10.0 km
Aerosol Model	3	MITR, WASO, COPO

ACPD
15, 7933–7975, 2015

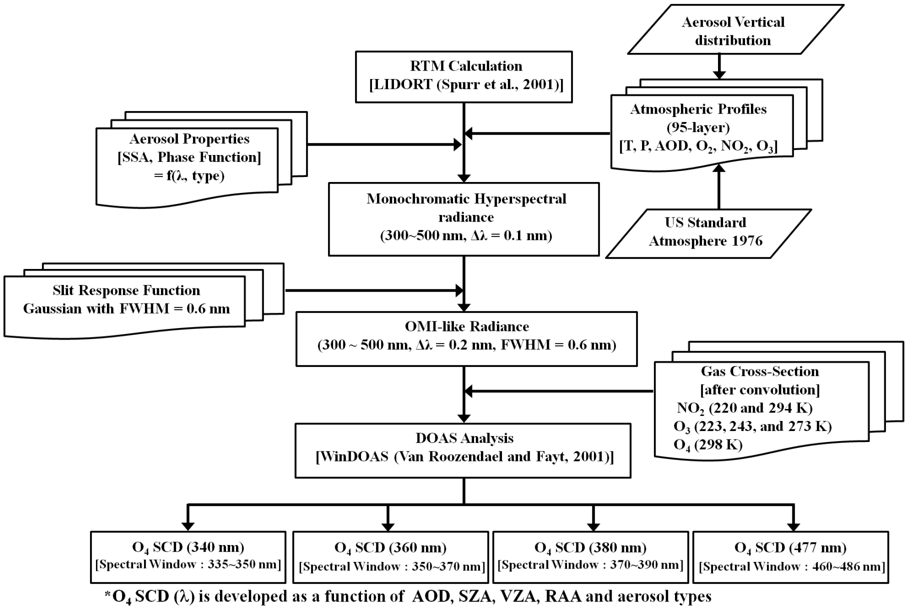

Figure 1. Flowchart of the simulated O_4 SCD estimation.

ACPD
15, 7933–7975, 2015

Utilization of O_4 slant column density to derive aerosol layer height

S. S. Park et al.

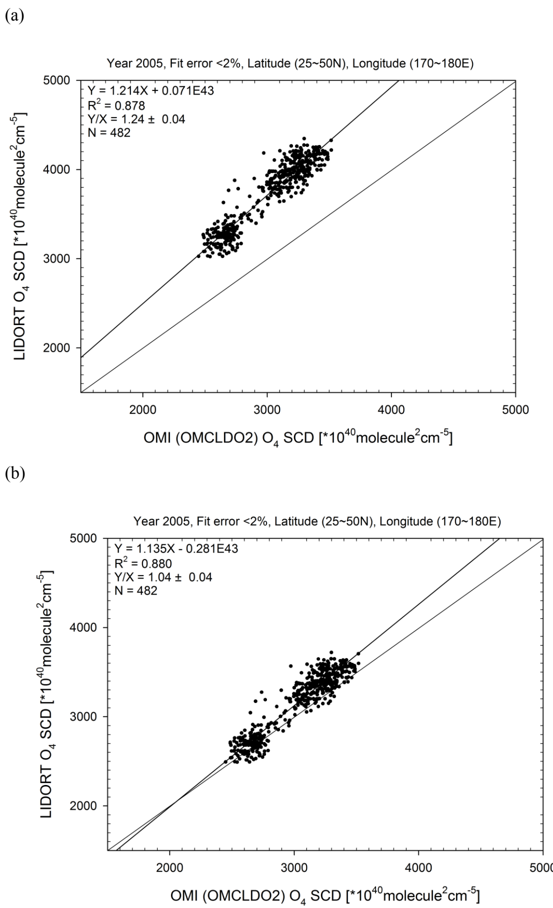

Figure 2. Comparison of the O_4 SCD at 477 nm between the standard product from OMI and calculated value from LUT **(a)** before and **(b)** after correction of O_4 cross section.

ACPD
15, 7933–7975, 2015

Utilization of O_4 slant column density to derive aerosol layer height

S. S. Park et al.

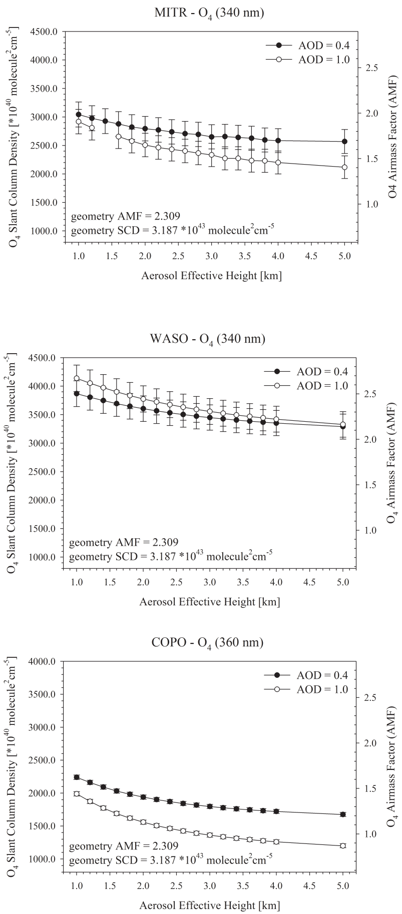

Figure 3. The O_4 SCD at 340 nm band for **(a)** MITR, **(b)** WASO, and **(c)** COPO as a function of AEH.

ACPD
15, 7933–7975, 2015

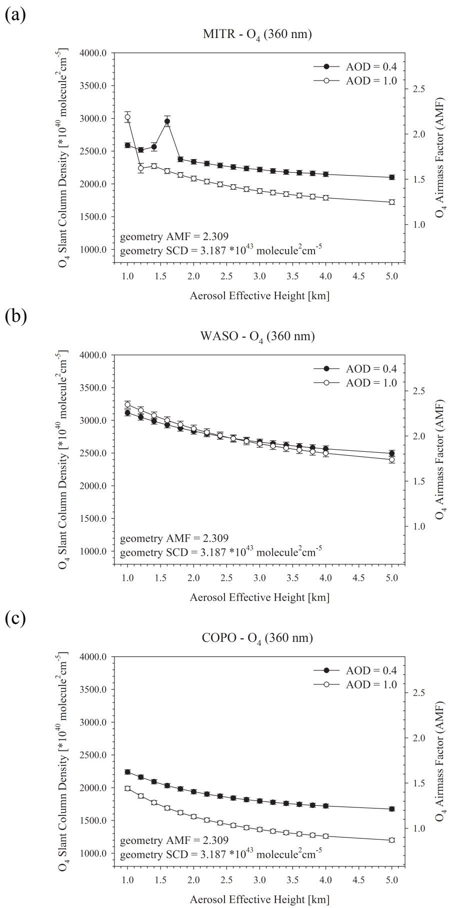

Figure 4. Same as Fig. 3 except for the O_4 SCD at 360 nm band.

ACPD
15, 7933–7975, 2015

Utilization of O_4 slant column density to derive aerosol layer height

S. S. Park et al.

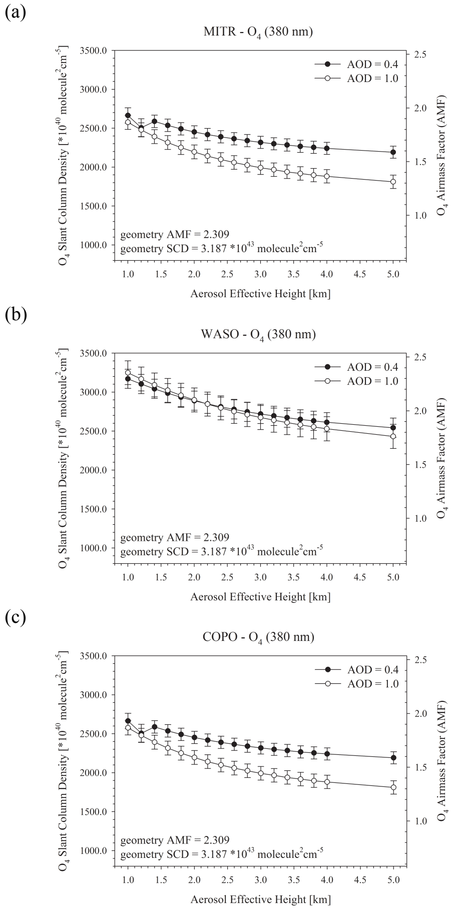

Figure 5. Same as Fig. 3 except for the O_4 SCD at 380 nm band.

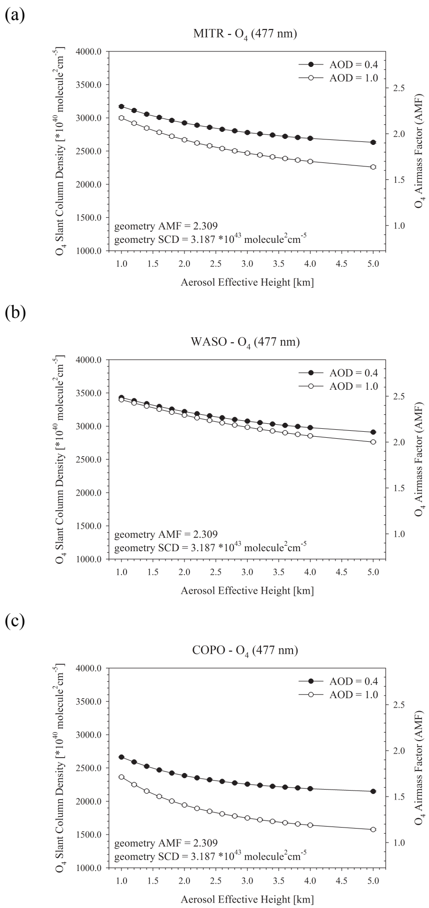

Figure 6. Same as Fig. 3 except for the O_4 SCD at 477 nm band.

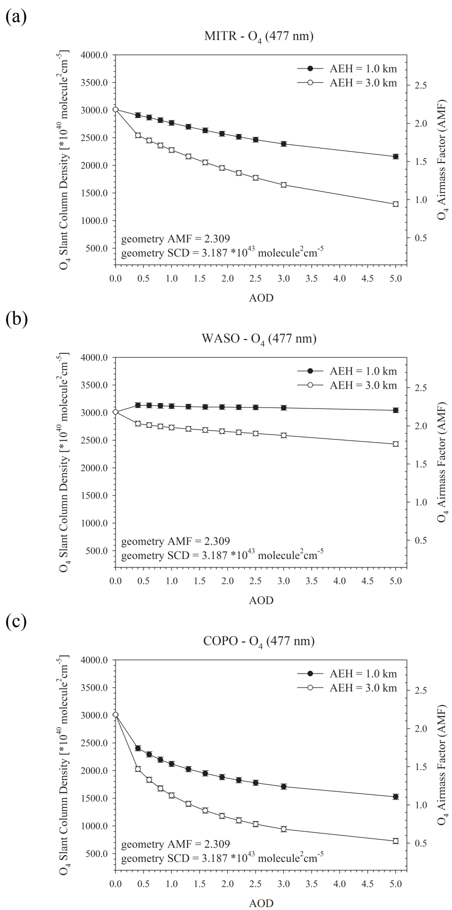

Figure 7. The O_4 SCD at 477 nm band of **(a)** MITR, **(b)** WASO, and **(c)** COPO types as a function of AOD.

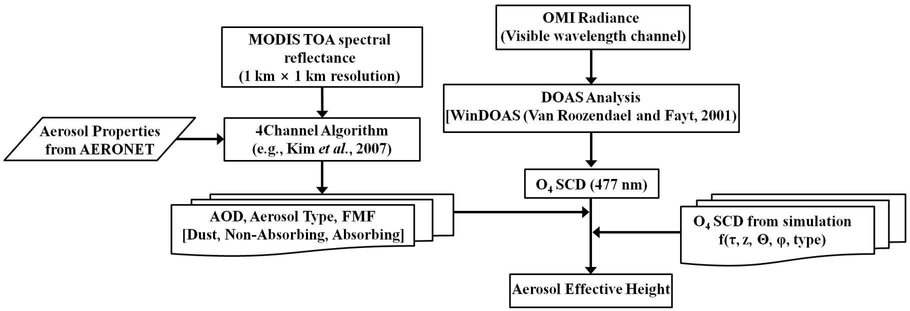

Figure 8. Flowchart of the retrieval algorithm for AEH using OMI radiance.

ACPD
15, 7933–7975, 2015

Utilization of O_4 slant column density to derive aerosol layer height

S. S. Park et al.

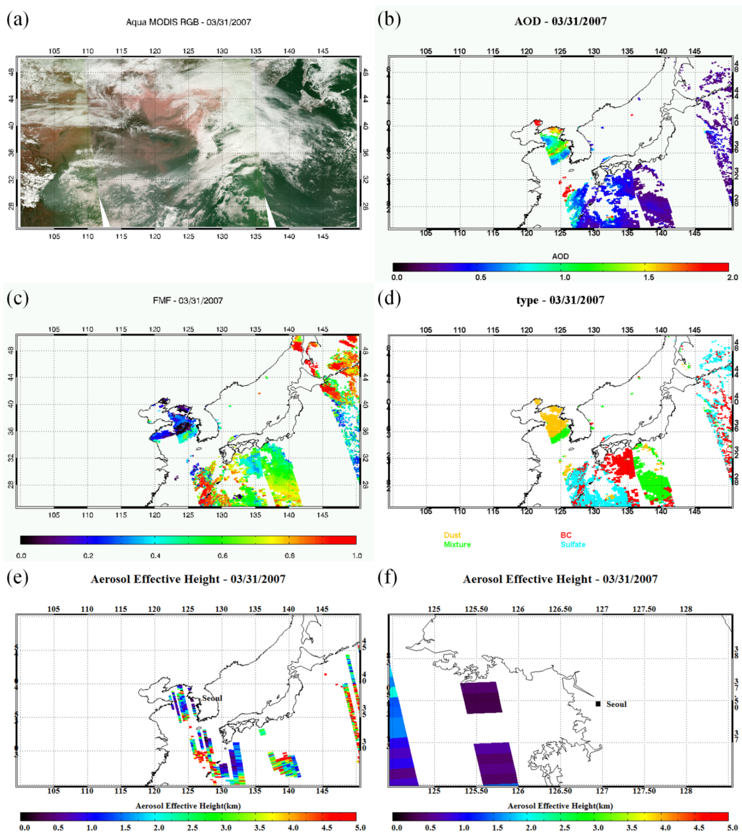

Figure 9. (a) MODIS RGB, **(b)** AOD, **(c)** FMF, **(d)** aerosol classification from 4CA, **(e)** AEH distribution from OMI over East Asia, **(f)** and AEH distribution near the lidar site at Seoul (Seoul National University, 37.45° N, 126.95° E, altitude: 118 m) on 31 March 2007.

ACPD
15, 7933–7975, 2015

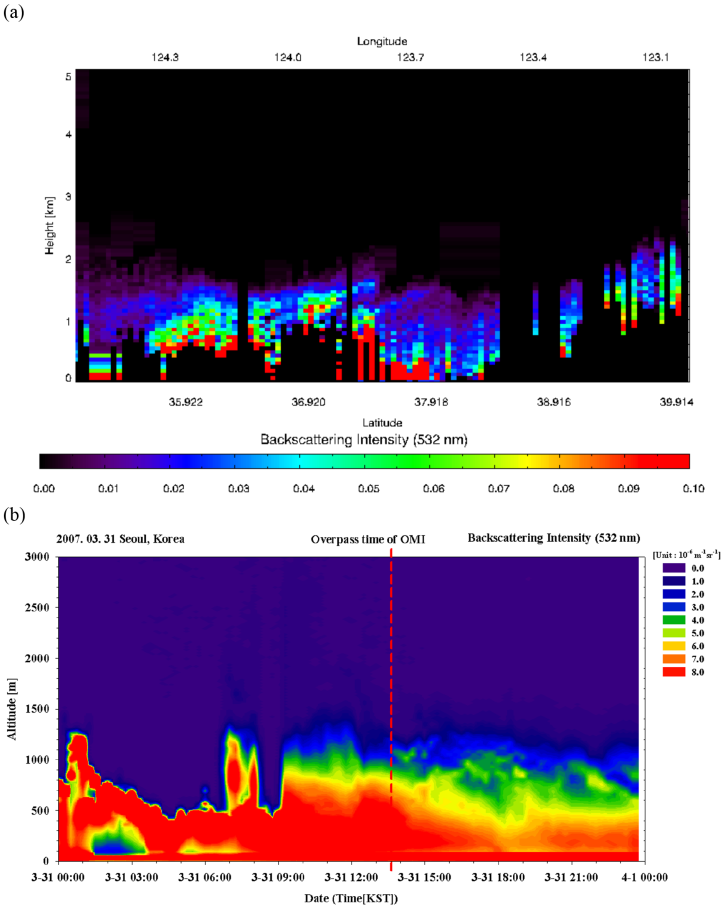

Figure 10. (a) Backscattering Intensity from CALIOP observation over Yellow Sea, and **(b)** those from LIDAR observation at Seoul site (Data Credit: National Institute for Environmental Studies, Japan) on 31 March 2007.